Green Chemistry

PAPER

View Article Online
View Journal | View Issue

Cite this: *Green Chem.*, 2025, **27**, 9937

Selective chemodivergent depolymerization of poly(cyclohexene carbonate) with lanthanide-organic catalysts†

Liwei Ye,[a] Xiaoyang Liu,[b] Giacomo Forti,[a] Linda J. Broadbelt,[*b] Yosi Kratish*[a] and Tobin J. Marks[*a]

If feasible, introducing chemodiversity into the selective chemical recycling of plastics would provide a resource- and catalyst-efficient means of recovering high-value building blocks from synthetic polymers for diverse recycling applications *via* straightforward alterations of catalytic conditions. Here we report the application of earth-abundant, readily available lanthanide-organic $Ln[N(TMS)_2]_3$ catalysts to the solventless chemodivergent, non-random back-biting depolymerization of poly(cyclohexenecarbonate) (PCHC) in high selectivity and near-quantitative conversion. Varying the lanthanide ionic radius across the 4f series and modifying the reaction conditions creates an efficient switch in PCHC depolymerization pathway to the corresponding epoxide (cyclohexene oxide; >99% selectivity; >94% yield) or the corresponding cyclic carbonate (*trans*-cyclohexene carbonate; >99% selectivity; 93% yield) monomer, each offering recycling value and closed-loop circularity. Combined experimental and theoretical DFT mechanistic analyses indicate two competing depolymerization pathways: low-energy reversible cyclic carbonate formation and rate-limiting irreversible decarboxylation. These catalysts are recyclable and applicable to plastics mixtures such as PCHC + nylon-6 + polyethylene, enabling sequential monomer capture with a single catalyst in the solvent-free process.

Received 20th March 2025,
Accepted 21st July 2025

DOI: 10.1039/d5gc01399b

rsc.li/greenchem

Green foundation

1. Poly(cyclohexene carbonate) (PCHC) is a sustainable CO_2-derived engineering polymer, yet conventional PCHC recycling often requires harsh conditions with little control over monomer selectivity. Here, we introduce the first application of earth-abundant tunable ionic radius lanthanide-organic catalysts that selectively converts PCHC into either of two different monomeric products, each capable of closed-loop chemical recycling: cyclohexene oxide (CHO) or *trans*-cyclohexene carbonate (*trans*-CHC), each delivering >99% purity and near-complete conversion.
2. This approach achieves a rare example of chemodivergence in polymer recycling, allowing precise control over monomer recovery. Additionally, it enables mixed plastic recycling by selectively depolymerizing and separating PCHC in the presence of other polymers, demonstrating its compatibility for real-world mixed-plastic waste recycling.
3. This work establishes a novel strategy for CO_2-based polymer recycling, demonstrating how catalyst-controlled depolymerization provides tunable monomer recovery. These findings can inspire future advancements in catalyst design for plastic recycling.

Introduction

Chemodivergent catalytic processes provide a unique, resource- and catalyst-efficient strategy for expanding product diversity from common starting materials,[1–4] making them ideal to address emerging challenges associated with environmental issues, such as plastics pollution. For decades, escalating concerns regarding plastics pollution have motivated the need for effective recycling technologies.[5–7] With 4.5×10^8 tons of plastics produced annually, great interest has been drawn to chemical recycling processes, which offer the opportunity to reclaim the monomeric units of polymers, thereby enabling closed-loop polymer circularity without compromising materials properties.[8,9] An important class of polymers is polycarbonates, which are high-performance thermoplastics widely used with a 2022 global market surpassing $22.6B.[10] Aromatic polycarbonates incur a significant production carbon footprint

[a]*Department of Chemistry, Northwestern University, and the Trienens Institute for Sustainability and Energy, Evanston, IL 60208-3113, USA.*
E-mail: t-marks@northwestern.edu
[b]*Department of Chemical and Biological Engineering, Northwestern University, and the Trienens Institute for Sustainability and Energy, Evanston, IL 60208-3113, USA.*
E-mail: broadbelt@northwestern.edu

† Electronic supplementary information (ESI) available. See DOI: https://doi.org/10.1039/d5gc01399b

and to date have eluded effective chemical recycling. In contrast, aliphatic polycarbonates prepared from epoxide/CO_2 ring-opening copolymerization are more attractive and have gained attention due to their capture of greenhouse CO_2, tunable properties, and chemical recyclability to monomers.[11–17]

Among aliphatic polycarbonates, poly(cyclohexene carbonate) (PCHC; Scheme 1A) is the most widely used CO_2-derived polycarbonate. While PCHC is still in the R&D stages, it shows significant promise as a sustainable engineering plastic, reflecting its optical transparency, high tensile strength, and excellent stability/ductility,[18,19] with significant potential in applications such as construction, electronics, automobile, eyewear, and medical equipment. PCHC has also served as a well-established literature benchmark for evaluating the activity and selectivity of aliphatic polycarbonate depolymerization catalysts.[8] The unique chemical recyclability of PCHC lies in its potential depolymerization to yield either of two different monomers: the 5-membered cyclic carbonate *trans*-cyclohexene carbonate (*trans*-CHC) and/or the corresponding epoxide, cyclohexene oxide (CHO), both of which can be repolymerized to pristine PCHC in closed-loop recycling (Schemes 1A and B).[8] Importantly, recovering either monomer offers distinct appeal: epoxides can be readily repolymerized or copolymerized into diverse high-value materials *via* effective upcycling;[20,21] cyclic carbonates find extensive utilization as aprotic solvents[22] or pharmaceutical intermediates,[23] and are often favored for sequestering greenhouse CO_2.[24]

Interest in the chemical recycling of PCHC has grown significantly in recent years (see ESI Fig. S1†) as a representative CO_2-derived sustainable polymer. This work demonstrated selective PCHC depolymerization to monomer CHO + CO_2 using well-optimized mono- or bimetallic catalysts (Scheme 1A),[25–29] while typically high-temperature PCHC pyrolysis processes (>250 °C) are most effective for the other monomer, *trans*-CHC, as reported by Coates *et al.* (Scheme 1B).[8,21,30,31] Challenges associated with CHO stem from the high kinetic barrier to epoxide formation, requiring elaborate catalyst structures,[32] exemplified by the pioneering studies of Williams *et al.* using heterodinuclear complexes for efficient CHO + CO_2 recovery. These include a dinuclear Mg(II) catalyst,[25] and heterodinuclear Mg(II)Co(II) catalysts for PCHC depolymerization under solventless conditions.[27,28] Lu *et al.* reported selective PCHC pyrolysis to CHO + CO_2 using a Cr(III)-Salen catalyst with a PPN-N_3 [bis(triphenylphosphine) iminium azide] cocatalyst at 200 °C.[26] While these mono-/dinuclear complexes demonstrate good activity and general selectivity, their preparation involves multiple synthesis/purification steps.

Lanthanide-based catalysts that play a significant role in chemical synthesis, are earth-abundant (La abundance in the earth's crust is comparable to that of Ni and Cu),[33] kinetically labile, highly electrophilic, structurally tunable, and usually readily available.[34–40] For example, $Ln[N(TMS)_2]_3$ complexes (**Ln^{NTMS}**) rapidly and selectively catalyze ketone and aldehyde,[41] ester,[36] as well as amide reductions,[42] and more recently were used in selective and Ln^{3+} radius-dependent polyester[43] and nylon-6 depolymerization.[44,45] This motivated us to investigate their potential in polycarbonate deconstruction.

Here we report the rapid, selective, and solventless depolymerization of PCHC using readily available **Ln^{NTMS}** model catalysts (Scheme 1C). While not the most active lanthanide-organic catalysts,[44,45] this series allows ready evaluation of Ln^{3+} ion size effects, kinetic/mechanistic selectivities, and DFT computational analysis, revealing two discrete and heretofore unrecognized competing depolymerization pathways to produce either of the two different PCHC monomers. An efficient chemodivergence is thereby realized, enabling selective recovery of CHO or *trans*-CHC by simply switching between depolymerization methodologies. Considering the intrinsic values of both monomers, such a catalytic approach is attractive for accessing different recycling/upcycling scen-

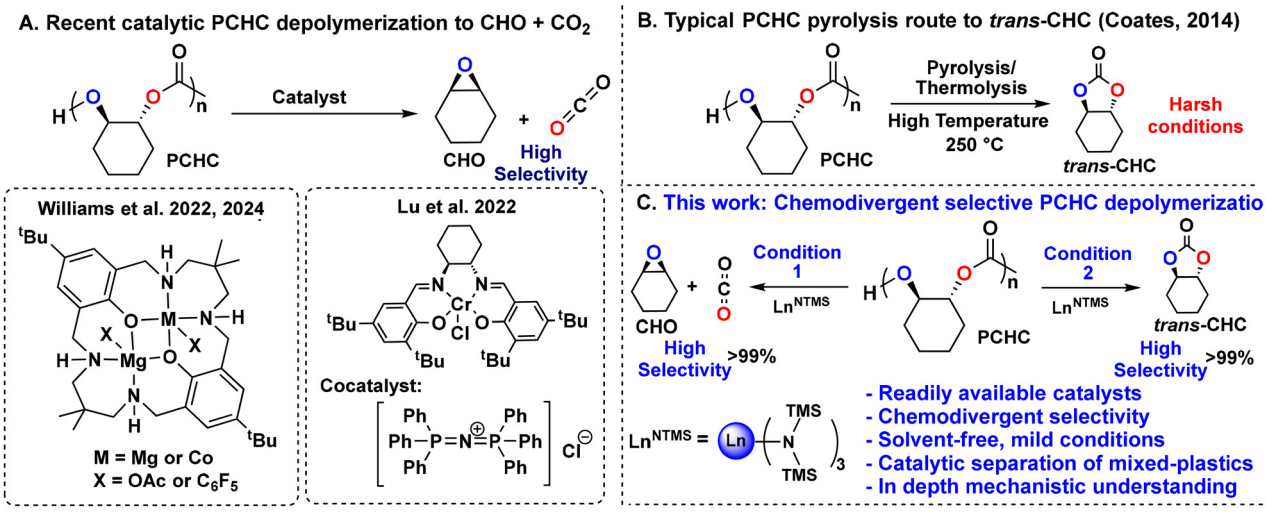

Scheme 1 Overview of PCHC depolymerization to monomers.

arios *via* straightforward modifications of reaction conditions. While strict Ln^{3+} size chemodivergence is observed in organolanthanide-mediated pyridine C–H borylation *vs.* dearomatization,[46] such an interplay between catalytic conditions and monomer selectivity in polymer depolymerization processes has never been previously, to our knowledge, achieved and with such selectivity.

Results and discussion

Catalyst screening: lanthanide ionic radius effects

Surprisingly, unlike typical base-initiated depolymerization of aliphatic PCs to the corresponding cyclic carbonates, **La^{NTMS}** catalyzes PCHC depolymerization to epoxide CHO in high selectivity (>99%) and conversion (93%) under static vacuum at 140 °C in 3 h (Table 1, entry 1). Despite the high basicity of the –NTMS ligands, cyclic carbonate *trans*-CHC, which is the expected product from PCHC *via* a ring-closing mechanism, is not observed, in contrast to the **La^{NTMS}**-catalyzed depolymerization of polyesters[33] and polyamides[34] which yield the corresponding cyclic lactones and lactams, respectively, and other base-mediated depolymerizations of CO_2-derived PCs.[30] This result suggests a unique catalytic role of the Ln^{3+} center.

Table 1 PCHC depolymerization data as a function of the metal ionic radius using **Ln^{NTMS}** and **Sc^{NTMS}** catalysts

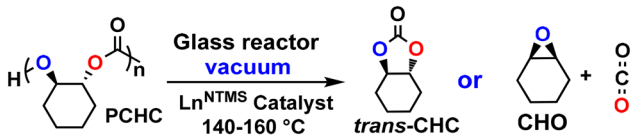

Entry[a]	Catalyst (Ln^{3+} ionic radius)	Total conv.[b] (%)	Monomer selectivity: *trans*-CHC[c] (%)	Monomer selectivity: CHO[c] (%)	TOF[e]: *trans*-CHC	TOF[e]: CHO
1	**La^{NTMS}** (1.030 Å)	93	—	>99	—	6.2
2	**Sm^{NTMS}** (0.960 Å)	62	25	75	1.03	3.1
3	**Lu^{NTMS}** (0.861 Å)	23	80	20	1.22	0.31
4	**Sc^{NTMS}** (0.745 Å)	8.5	93	7	0.53	0.04
5	No catalyst	<1	>99	—	—	—
6[d]	**La^{NTMS}** (1.030 Å)	93	>99	—	55.8	—

[a] Unless otherwise noted, reactions were performed solventless with 100 mg PCHC under static vacuum in a closed 50 mL Schlenk tube with 5 mol% catalyst at 140 °C for 3 h. See ESI† for details. [b] From integrating ^{1}H NMR of *trans*-CHC (3.0 ppm) + CHO (2.8 ppm) *vs.* PCHC (4.7–5.0 ppm) reaction mixture in d^8-toluene. Note PCHC signals appear as broad features in the 4.6–4.8 ppm range, consistent with literature data.[25,27]. [c] Product distribution assayed by ^{1}H NMR. [d] Under dynamic vacuum, 160 °C, 20 min. [e] Estimated TOF (turnover frequency) in units of (mol of monomer) (mol Cat.)$^{-1}$ (h)$^{-1}$.

To further investigate Ln^{3+} effects on the current system, a series of homoleptic **Ln^{NTMS}** precatalysts where Ln = La, Sm, Lu, and Sc was surveyed under identical solventless, mild depolymerization conditions and static vacuum (Table 1, entries 2–4). Note that under the same reaction conditions, contraction of the Ln^{3+} ion radii alters PCHC depolymerization selectivity and rate: large La^{3+} exclusively favors rapid epoxide formation, Sm^{3+} yields mixed products, Lu^{3+} predominantly yields *trans*-CHC, and small Sc^{3+} favors exclusive cyclic carbonate formation (*trans*-CHC) at low conversion. Control experiments without a catalyst under identical conditions yield only traces (<1%) of the thermodynamically favored[31] *trans*-CHC product (Table 1, entry 5). This demonstrates a significant catalytic role for the **Ln^{NTMS}** complexes at this reaction temperature (140–160 °C), with non-catalytic PCHC thermolysis requiring a far higher temperature (250 °C).[31]

Kinetic studies

Considering the apparent dependence of monomer selectivity on the metal ionic radius, combined with a fall in conversion rate as the Ln^{3+} ionic radius contracts from La^{3+} (1.030 Å) to Sc^{3+} (0.745 Å), we hypothesized that *trans*-CHC may play an intermediate role in the reaction pathway. To probe this hypothesis, kinetic studies (Fig. 1A) were performed to monitor *trans*-CHC *vs.* CHO product distribution over the course of the 0–3 h reaction using the most active and a moderately active catalyst (Table 1, entries 1 and 2). The data indicate that *trans*-CHC is predominantly produced in the initial stages of reaction, followed by a gradual increase in the CHO monomer content, eventually reaching >99%. We further hypothesized that in a closed reaction system, *trans*-CHC might further undergo conversion to CHO + CO_2 mediated by **Ln^{NTMS}**.

To investigate whether the **Ln^{NMTS}**-catalyzed PCHC depolymerization proceeds *via* a back-biting mechanism from hydroxyl end groups or *via* random chain scissions, total monomer conversion (*trans*-CHC + CHO) was plotted *versus* time (Fig. 1B). A linear increase in monomer yield is observed over the first 30 min (up to ~63%), followed by saturation. This behavior indicates that the reaction is initially zero-order in [PCHC], suggesting that in the catalyst resting state the polymer is bound to the La center largely at the chain end and depolymerization proceeds with the catalyst walking along the chain. Saturation presumably reflects PCHC depletion and/or catalyst deactivation at chain ends. This kinetic behavior closely resembles profiles previously we previously reported for Nylon-6 depolymerization with Ln-based catalysts.[34,35]

Gel Permeation Chromatography (GPC) analysis was also used to examine polymer MW at 0–1.5 h reaction times. The results show a gradual decrease in MW (Fig. S7†), supporting a back-biting mechanism in which monomers are sequentially eliminated from the polymer chain end in each catalytic cycle, although the observed increase in polydispersity as the reaction progresses may suggest some presence of a competing random scission mechanism.

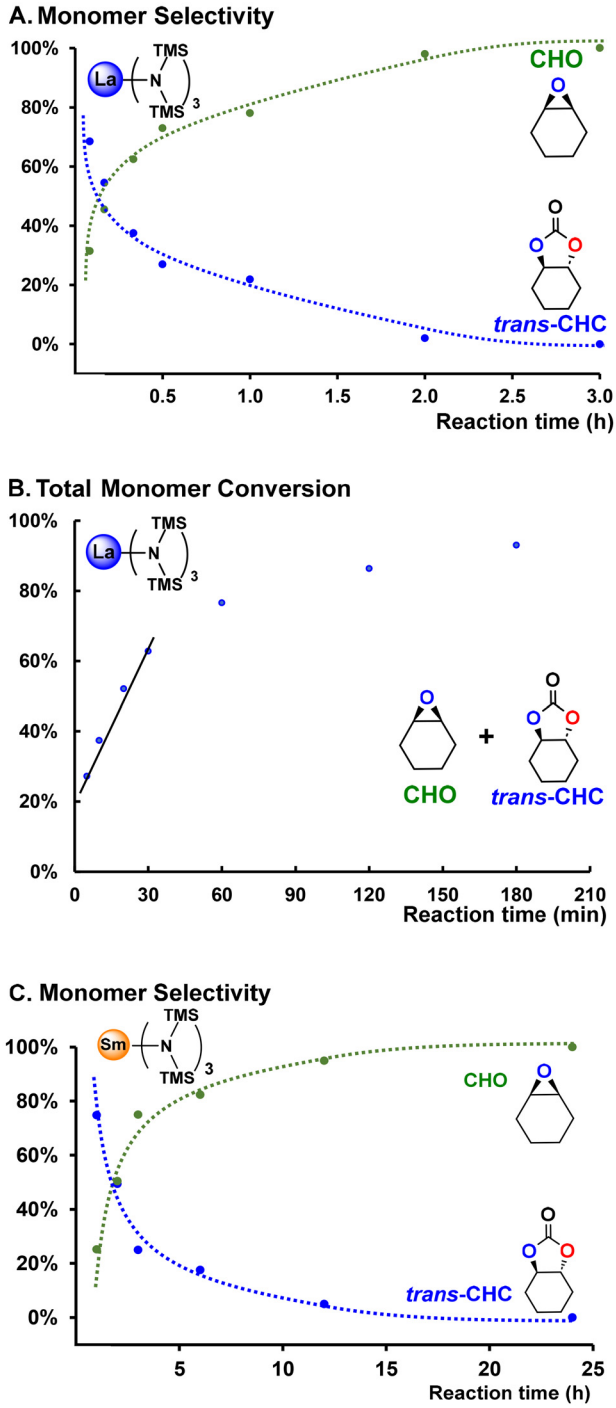

Fig. 1 A. Kinetic profile of PCHC depolymerization in a closed reaction system using La^{NTMS} under the conditions of Table 1. B. Total monomer conversion (*trans*-CHC + CHO) *versus* reaction time. C. Kinetic profile of PCHC depolymerization in a closed reaction system using Sm^{NTMS}.

The respective conversions of CHO and *trans*-CHC *vs.* time were plotted (Fig. S8 and S9†). The data reveal that the quantity of *trans*-CHC remains relatively constant at a low level (~15–20%) during the early stages of the reaction, followed by the eventual decrease to 0% by the end of the 3-hour kinetic study. Parallel kinetic studies with Sm^{NTMS} reveal that for the smaller Ln^{3+} ionic radius, a similar CHO selectivity (>99%) is achieved, albeit with a slower approach to equilibrium (Fig. 1C).

Mechanistic studies: *trans*-CHC reactions

To further probe the reaction pathway and understand the origin of Ln^{NTMS} product selection, *trans*-CHC was synthesized separately and exposed to several Ln^{NTMS} catalysts under identical depolymerization conditions (Table 2), testing the hypothesis that these catalysts should mediate CHO formation and at different rates. In agreement with the findings in Table 1, Ln^{NTMS} catalysts having larger ionic radii are more active decarboxylation catalysts for CHO formation (Table 2; La^{NTMS} > Sm^{NTMS} > Lu^{NTMS} > Sc^{NTMS}). Importantly, all of these Ln^{NTMS} catalysts are active in *trans*-CHC polymerization to PCHC, indicating a likely reversible pathway from PCHC to *trans*-CHC depolymerization. Note that in Table 1, depolymerization reactions, the 50 mL Schlenk flask provides a large upper cold zone area for CHO condensation/collection, thus displacing the equilibrium towards quantitative CHO formation in >99% selectivity in entry 1 with La^{NTMS}. Interestingly, smaller Ln^{3+} ionic radii Ln^{NTMS} complexes are more active polymerization catalysts and less active decarboxylation catalysts. Sc^{NTMS}, as the smallest group 3 ion, affords only trace CHO product, in good agreement with its sluggish PCHC depolymerization rate (Table 1).

Chemodivergence in PCHC depolymerization selectivity

Intrigued by the above results, we find that *trans*-CHC is indeed converted to CHO and CO_2, but not *via* direct decarboxylation. Instead, *trans*-CHC first undergoes re-polymerization to PCHC (see results in Table 2), which is then depolymerized to CHO and CO_2. Furthermore, employing a continuous vacuum and a cold trap might allow isolation of *trans*-

Table 2 Product distributions after 3 h for reactions of *trans*-CHC using the indicated amido catalysts[a]

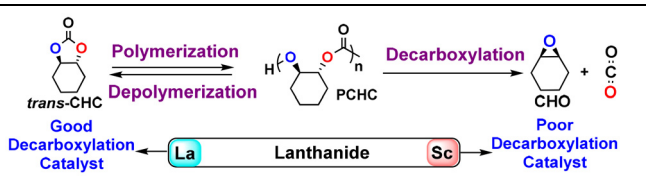

Catalyst	*trans*-CHC (reagent)	PCHC (polymerization)	CHO (decarboxylation)
La^{NTMS}	6%	40%	54%
Sm^{NTMS}	15%	38%	47%
Lu^{NTMS}	24%	69%	7%
Sc^{NTMS}	28%	71%	1%

[a] Conditions: reactions performed solventless with 100 mg *trans*-CHC under static vacuum conditions in a closed 5 mL Schlenk tube. The reactor is completely submerged in an oil bath at 140 °C for 3 h. Product distributions determined from the ^{1}H NMR integrals of *trans*-CHC (3.0 ppm) + CHO (2.8 ppm) *vs.* PCHC (4.7–5.0 ppm).

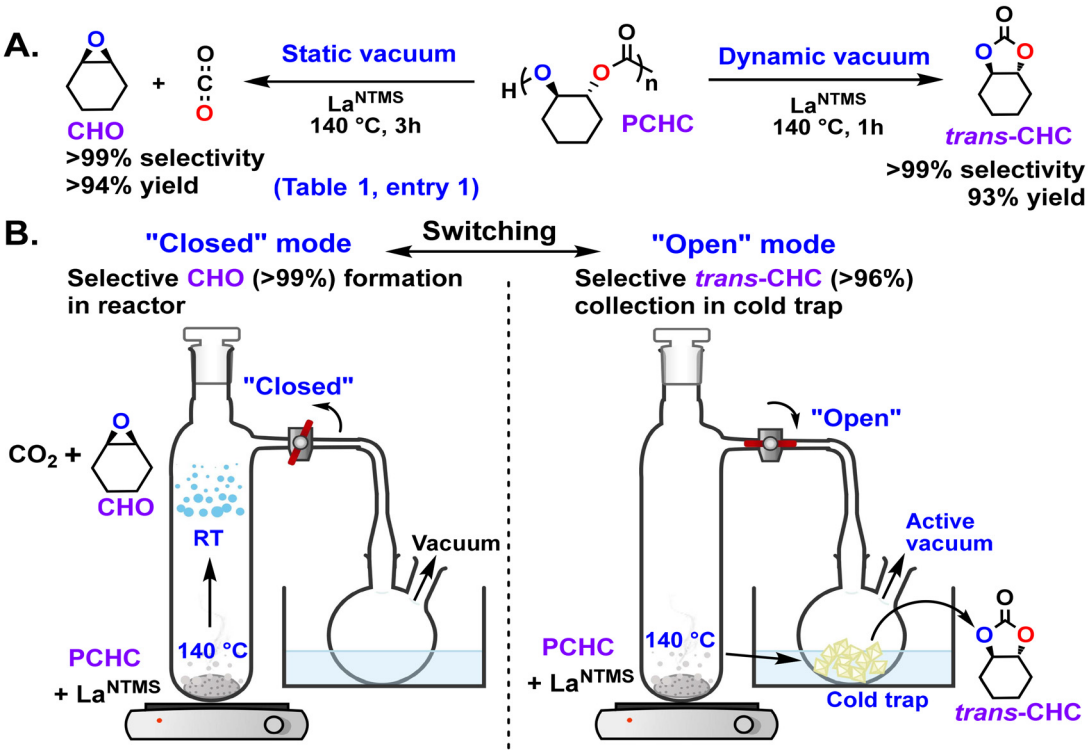

Fig. 2 A. Chemodivergent effects of reactor configuration on monomer selectivity in PCHC depolymerization. B. Reactor configured in switchable "Open" and "Closed" modes to yield their respective chemodivergent monomers in high yield and selectivity.

CHC, preventing further conversion. Strikingly, when the reaction methodology in Table 1, entry 1 is altered from a closed Schlenk reactor to a reactor under dynamic vacuum, the monomer selectivity of the **La^{NTMS}**-catalyzed PCHC depolymerization is completely reversed (Fig. 2A), with the reaction affording *trans*-CHC selectively (>99%) with high conversion (93%) in only 1 h at 140 °C (see Table 1, entry 6 and Table S1,† entry 1). The reaction is rapid at 160 °C to reach a 94% yield of *trans*-CHC in only 20 min using 5 mol% **La^{NTMS}**, while a lower catalyst loading (1 mol%) achieves full conversion of *trans*-CHC in 3 h (Table S1,† entries 2 and 3).

To demonstrate that this chemodivergent monomer selectivity is a truly "switchable" **La^{NTMS}**-catalyzed phenomenon, a reactor was employed (Fig. 2B and Fig. S15†) having a valve linking a Schlenk reactor and a cold trap. When the reactor is in "Open" mode (valve opened), *trans*-CHC is collected in the cold trap under active vacuum with >96% selectivity at 99% conversion. However, when the reactor is switched to "Closed" mode, CHO is formed in the Schlenk tube in >99% selectivity at 96% conversion, consistent with the data in Table 1, entry 1. These results present an unusual example in the field of plastics depolymerization/recycling in which the same catalyst and reaction conditions afford two different polymerizable monomers in high purity and conversion by simply switching between static and dynamic vacuum. Given the distinctive utility of both the present monomers, this chemodivergent catalytic approach offers an intriguing solution for different recycling and upcycling options *via* straightforward adjustments in depolymerization conditions.

Solventless catalytic separation of mixed-plastics

Since **La^{NTMS}** is also effective for catalytic Nylon-6 depolymerization,[34] we were intrigued by the possibility of catalytically separating plastics mixtures *via* a simple variation of reaction modality (Scheme 2). Thus, for a mixture containing 250 mg each of PCHC + Nylon-6 + polyethylene in a sublimation reactor, PCHC was first selectively depolymerized to clean *trans*-CHC at 140 °C in 74% isolated yield. Note that ε-caprolac-

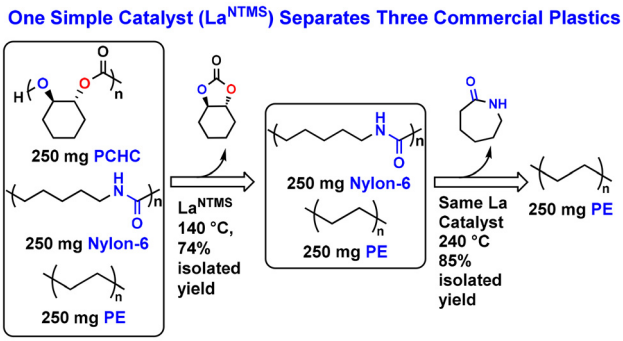

Scheme 2 La^{NTMS} mediates the clean catalytic separation of PCHC + Nylon-6 + PE mixtures.

tam is not obtained at this temperature, consistent with the inertness of Nylon-6 + $\mathbf{La^{NTMS}}$ at this relatively low temperature. Next, after collection of the *trans*-CHC, the reaction temperature is elevated to 240 °C (no catalyst addition), rapidly depolymerizing the Nylon-6 to ε-caprolactam in 85% isolated yield in 3 h, leaving the residual polyethylene unchanged. Separating PCHC by converting to CHO + CO_2 from a mixed-plastic system was also attempted, although clean conversion of the desired reaction in the presence of nylon-6 and polyolefins is not achieved (~40% of *trans*-CHC still remains, see ESI† page 20). We attribute this limitation to reduced mass transfer and poorer contact between the formed *trans*-CHC and the catalyst in the solid mixture, which hinders the necessary re-entry of *trans*-CHC into the catalytic cycle.

This model experiment reflects the broad and tunable scope of the inherently cost-effective and readily accessible lanthanide-organic catalysis for polymer recycling and commodity plastics mixture separation. These results highlight not only the recyclability of the catalyst but also its stability and versatility under the reaction conditions. Its ability to promote multiple depolymerization reactions without reactivation shows its robustness and practical utility in chemical recycling. Notably, the only detectable contamination in the recovered monomers originates from the $(TMS)_2NH$ ligand, which possesses a lower boiling point than either product and can be readily removed by distillation.

DFT mechanistic analysis

To further probe the origin of the present chemodivergent effects, the mechanism of the $\mathbf{La^{NTMS}}$-catalyzed PCHC depolymerization was probed using density functional theory (DFT) to compare and contrast possible reaction pathways, as illustrated in Fig. 3 (see ESI† for details). The α,ω-hydroxy telechelic PCHC (PCHC-OH) monomer was selected as the model to simulate the chain-end initiated depolymerization mechanism, as also proposed for PCHC depolymerization using dinuclear catalysts by Williams *et al.*[25] Chain-end unzipping *vs.* random scission mechanisms were also investigated by DFT calculations using both La-NTMS and La-OR potential active species (Fig. S19 and S20†). Results show that in both

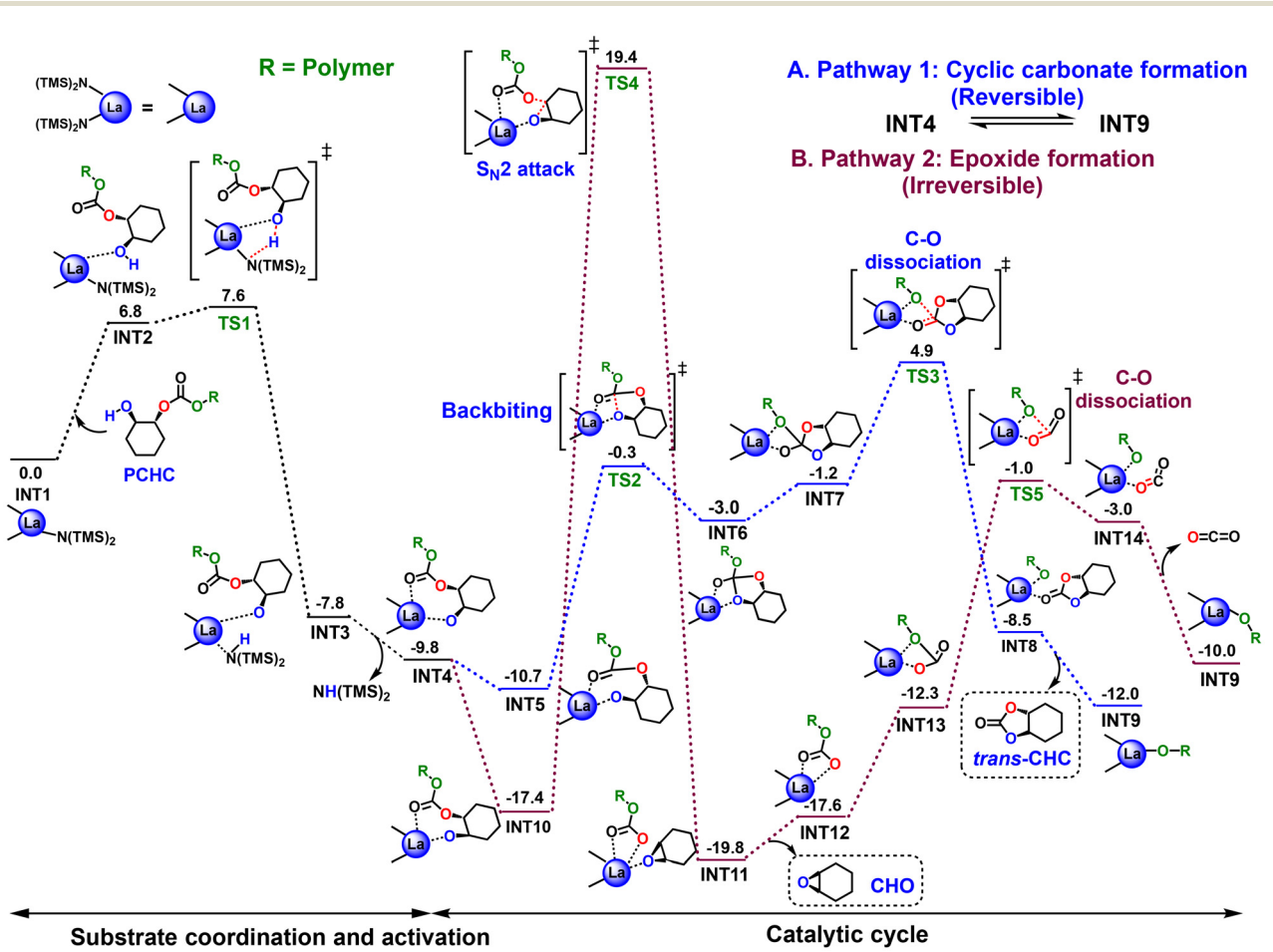

Fig. 3 DFT-derived Gibbs free energy profile for the catalyst coordination and activation step, and $\mathbf{La^{NTMS}}$-catalyzed PCHC depolymerization cycle including two competing pathways A. Cyclic carbonate (*trans*-CHC) formation (blue dotted lines) B. Epoxide (CHO) and CO_2 formation (maroon dotted lines). Values were calculated at 140 °C in kcal mol^{-1} at the PBE0-D3BJ/def2-TZVP//PBE0-D3BJ/def2-SVP[47–52] level of theory, incorporating the SMD solvation model[53] of ethylactetate (ε = 5.9867). R = methyl for the calculation.

cases, chain-end unzipping is more kinetically favorable than mid-chain scission. The catalyst-**PCHC** coordination and activation step, which involves La^{3+}-oxygen binding (from **INT1** to **INT2**) followed by proton transfer from PCHC to the –NTMS ligand *via* **TS1** leads to **INT3**, resembling steps that we mapped in Nylon-6 depolymerization.[34,35] Next, the dissociation of HN$(TMS)_2$ leads to **INT4**, which initiates the catalytic depolymerization cycle(s). Then, two competing pathways for PCHC depolymerization are examined, with **Pathway 1** producing *trans*-CHC and **Pathway 2** producing CHO + CO_2.

Pathway 1 (Blue dotted line). From **INT4**, the polymer undergoes relaxation to **INT5** followed by a two-step addition–elimination reaction (through **TS2** and **TS3**) to generate *trans*-CHC *via* a "back-biting" process. Note that similar back-biting mechanisms have been proposed in the literature for the depolymerization of various CO_2-derived polycarbonates.[21,30] The ΔG for the addition step **INT5** → **INT6** is computed to be 7.8 kcal mol^{-1} with $\Delta G^{\ddagger}$ = 10.5 kcal mol^{-1} (**TS2**), while the C–O dissociation step (**INT7** → **INT8**) is exergonic with ΔG = −7.4 kcal mol^{-1} and $\Delta G^{\ddagger}$ = 6.0 kcal mol^{-1}. This is followed by the release of *trans*-CHC and formation of **INT9** (ΔG = −3.5 kcal mol^{-1}). The overall computed reaction barrier for **Pathway 1** is 15.6 kcal mol^{-1} (**INT5** → **TS3**). However, **INT5** is not the lowest energy intermediate, and as discussed below, the kinetics of **Pathway 1** will be guided by the stability of an intermediate that lies along **Pathway 2** where, from **INT4**, the structure can relax to form **INT10**, yielding a net free energy barrier of 22.3 kcal mol^{-1}.

Pathway 2 (Red dotted line). From **INT10**, an S_N2 attack occurs at an adjacent unit *via* **TS4** (ΔG = −2.4 kcal mol^{-1}; $\Delta G^{\ddagger}$ = 36.8 kcal mol^{-1}). This is followed by the release of monomeric CHO and the transition to **INT12** and **INT13**. Subsequent cleavage of the C–O bond *via* **TS5** then yields **INT14** (ΔG = 9.3 kcal mol^{-1}; $\Delta G^{\ddagger}$ = 11.3 kcal mol^{-1}), followed by CO_2 release. The formation of CHO and CO_2 occurs with ΔG values of 2.2 kcal mol^{-1} and −7.0 kcal mol^{-1}, respectively. Note that both pathways conclude with **INT9**, where R denotes the remainder of the polymer chain, and this structure can re-enter the catalytic cycle as **INT4**. The overall computed reaction barrier for **Pathway 2** is 36.8 kcal mol^{-1} (**INT10** → **TS4**). In comparing these two pathways, both of which proceed from **INT4** to **INT9**, the lower energy barrier of **Pathway 1** *vs.* **Pathway 2** ($\Delta G^{\ddagger}$ = 22.3 *vs.* 36.8 kcal mol^{-1}, respectively) indicates kinetically more favorable *trans*-CHC formation. Furthermore, note that the formation of *cis*-CHC from **Pathway 2** is kinetically less favorable compared to CO2 release (Fig. S21†). Additionally, **INT4**, **INT5**, and **INT10** are interchangeable isomeric configurations, with **INT10** being the most stable intermediate, which affects the rates of both **Pathways 1 and 2**. Moreover, **Pathway 1** is found to be a reversible catalytic process with the reverse reaction (**INT9** → **INT4**) featuring an accessible energetic barrier for the rate-determining step (16.9 kcal mol^{-1}; $\Delta G^{\ddagger} = G_{TS3} - G_{INT9}$). This is in good agreement with our observation in Table 2 that the reverse of **Pathway 1** eventually leads to the polymerization of *trans*-CHC to PCHC.

Note that while *trans*-CHC is often considered an intermediate decomposing to CHO and CO_2 as proposed by other authors,[26,30] this study reveals its ability to repolymerize to PCHC in a closed system before further depolymerizing *via* **Pathway 2** (see Fig. 2). This alternative pathway is distinctly different from others and, to the best of our knowledge, represents the first instance for the catalytic recycling of CO_2-based PCs. These computational results align well with the intriguing chemodivergent selectivity demonstrated in Fig. 2. Under an active vacuum, *trans*-CHC generated *via* kinetically

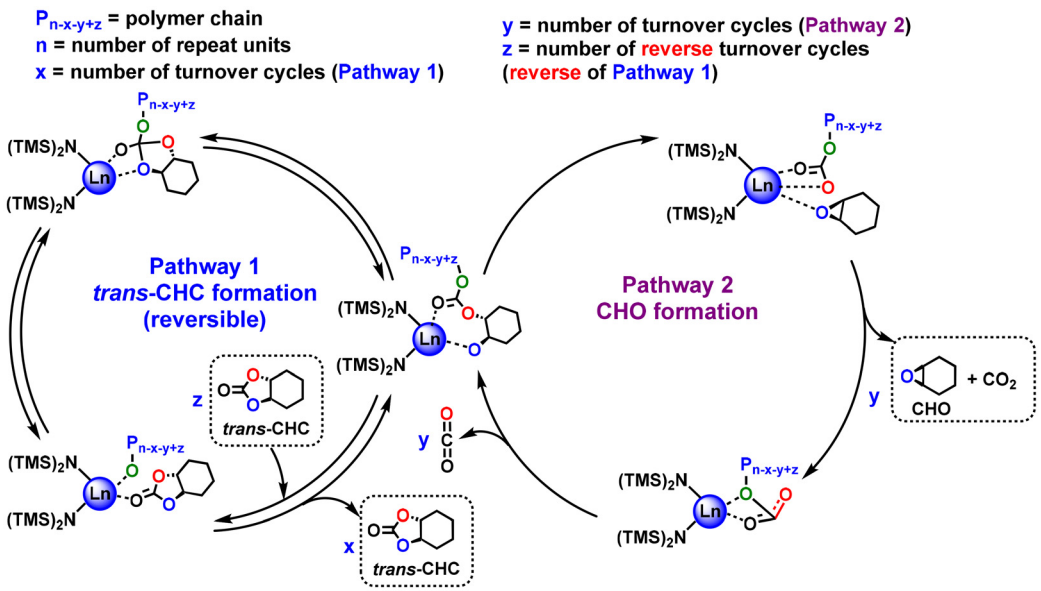

Fig. 4 Simplified dual catalytic cycles for the catalytic depolymerization of PCHC *via* two competing pathways.

favored **Pathway 1** is isolated and removed from the catalytic cycle, preventing the reverse reaction to **INT4** (Fig. 4). This further inhibits any CHO formation *via* **Pathway 2** under these conditions, in agreement with the high *trans*-CHC selectivity. Conversely, under static vacuum conditions where the *trans*-CHC product is not removed and can re-enter the catalytic cycle in the closed system, the DFT results suggest that the reverse of **Pathway 1** may occur to produce CHO *via* an **INT9** → **INT4** → **Pathway 2** mechanism, in agreement with the present kinetic information in Fig. 1. **Pathway 2** is irreversible since the polymerization of epoxides requires excess CO_2 to yield aliphatic PCs.[11,21,31] Note that the depolymerization of PCHC to CHO and CO_2 *via* **Pathway 2** is also strongly favored entropically, primarily driven by the removal of gaseous CO_2 to shift the reaction equilibrium, a key factor that is not fully captured by DFT,[25] due to the inaccuracy of using the qRRHO approximation to describe the entropy of adsorbed species[54,55] and the limitations of the implicit solvent model for computing solution-phase Gibbs free energies.[56] Furthermore, the calculations imply that **INT11**, which leads to CHO, is −11.4 kcal mol^{-1} more favorable than the intermediate that forms *trans*-CHC (**INT8**). This difference in energetic stability may also provide a substantial driving force for the formation of CHO mediated by $\mathbf{La^{NTMS}}$. These DFT results closely align with the present kinetic studies, which clarify the equilibrium dynamics in a three-component system (PCHC, *trans*-CHC, and CHO), and that a constant equilibrium is reached for *trans*-CHC throughout the entire process (see Fig. 1A, B and Fig. S12, S13†).

Conclusions

We report the solventless and selective depolymerization of PCHC using readily available model $\mathbf{Ln^{NTMS}}$ catalysts. Interestingly, $\mathbf{La^{NTMS}}$ with the largest Ln^{3+} ionic radius participates in the unique chemodivergent monomer selection for PCHC depolymerization in high conversions and rates: dynamic vacuum selectively affords *trans*-CHC (>99% purity at high conversions), while in a closed reaction system, CHO is produced in high selectivity (>99%) and conversion. This chemodivergent PCHC depolymerization selectivity, enabled by a 'switchable' reaction apparatus, provides facile selection of the desired monomer. In addition, this catalytic process can be adapted for the separation of commodity plastics mixtures containing PCHC, nylon-6, and polyethylene in a single-reactor solventless approach, leveraging the versatility of $\mathbf{La^{NTMS}}$ in selectively depolymerizing PCHC and nylon-6 to their respective monomers under orthogonal conditions. Regarding the mechanism, the experimental and theoretical analyses reveal a critical role of *trans*-CHC to re-enter the catalytic cycle *via* a reverse depolymerization pathway, followed by a kinetically more challenging/entropically more favorable CHO formation pathway. Furthermore, we find that while larger Ln^{3+} ions favor selective CHO formation in a closed system, smaller Ln^{3+} ions/early transition metal ions favor selective *trans*-CHC formation due to the unfavorable decarboxylation step as the $\mathbf{Ln^{NTMS}}$ ionic radius contracts. These mechanistic insights highlight the critical role of depolymerization conditions and lanthanide ion identity characteristics in dictating the reaction pathways and outcomes of the depolymerization processes. This knowledge should guide and advance the design of future catalytic processes for selective transformations in plastics recycling.

Experimental

Materials and methods

$\mathbf{La^{NTMS}}$, $\mathbf{Sm^{NTMS}}$, $\mathbf{Lu^{NTMS}}$, and $\mathbf{Sc^{NTMS}}$ were purchased from commercial sources and used after purification by recrystallization from pentane. Poly(cyclohexene carbonate) (PCHC) was obtained from Empower Materials (molecular weight range from 150 000 to 200 000, see Fig. S23† for its ^{1}H NMR spectrum). All polymers were ground to fine powders and dried under a high vacuum at 60 °C for at least 24 h prior to use. Note that the removal of residual moisture from polymer samples is critical to ensure optimal performance in the depolymerization reactions.

Physical and analytical methods

NMR spectra were recorded on a Varian Bruker Avance III HD system equipped with a TXO Prodigy probe (500 MHz) spectrometer. Chemical shifts (δ) for ^{1}H NMR are referenced to the internal solvent.

General procedure A. Depolymerization Reactions under static vacuum (see Fig. S24† for example). In an Argon-filled MBraun glovebox, a 50 mL oven-dried Schlenk tube was charged with a magnetic stir bar, PCHC powder, catalyst, and 2–3 mL of dry toluene. The vessel was sealed tightly, and the polymer and catalyst were thoroughly mixed and dissolved in toluene by stirring at room temperature for approximately 10 min. The Schlenk tube was then carefully evacuated to remove the toluene, sealed to maintain a static vacuum, and heated to the specified temperature with slow magnetic stirring (50–100 rpm) for the specified time. Heating was supplied by a customized aluminum heating block with a fitted hole or by an oil bath for the Schlenk tubes. During the reaction, the products sublime from the hot reaction zone and deposit as liquids on the cold wall of the reactor. After cooling to room temperature, the entire reaction mixture (including products on the cold region and any remaining solid mixture at the bottom of the flask) was dissolved in 3–4 mL of d^8-toluene with appropriate sonication. A sample of this solution was withdrawn for NMR analysis. Product distributions and conversions were determined by ^{1}H NMR, based on the relative ratios between the integrals for *trans*-CHC (3.0 ppm), CHO (2.8 ppm), and PCHC (4.5–5.0 ppm).

General procedure B. Depolymerization Reactions under dynamic vacuum (see Fig. S25† for example). In an Argon-filled MBraun glovebox, a sublimer was charged with a magnetic stir bar, PCHC powder, catalyst, and 2–3 mL of dry

toluene. The sublimer was sealed tightly, and the polymer and catalyst were thoroughly mixed and dissolved in toluene by stirring at room temperature for approximately 10 min. The sublimer was then carefully evacuated to remove toluene and heated to the specified temperature with slow magnetic stirring (50–100 rpm) for the specified time. Heating was supplied by an oil bath. The cold finger of the sublimator was cooled to −78 °C using a dry ice/acetone mixture. After cooling to room temperature, the entire reaction mixture (including products on the cold finger and any remaining solid mixture at the bottom of the sublimator) was dissolved in 3–4 mL of d^8-toluene with appropriate sonication. A sample of this solution was withdrawn for NMR analysis. Product distributions and conversions were determined by ^{1}H NMR, based on the relative ratios between the integrals for *trans*-CHC (3.0 ppm), CHO (2.8 ppm), and PCHC (4.5–5.0 ppm).

Conflicts of interest

There are no conflicts to declare.

Data availability

The authors confirm that the data supporting the findings of this study are available within the article [and/or] its ESI.†

Acknowledgements

The support of RePLACE (Redesigning Polymers to Leverage A Circular Economy), funded by the Office of Science of the U.S. Department of Energy *via* award no. DR-SC0022290 is acknowledged (L. Y., Y. K., T. J. M.). L. Y. also acknowledges support by National Science Foundation CAT f-element homogeneous catalysis grant CHE-2247666. L. J. B. also acknowledges BioOptimized Technologies to keep Thermoplastics out of Landfills and the Environment (BOTTLE) Consortium, supported by Advanced Materials and Manufacturing Office (AMMTO) and Bioenergy Technologies Office (BETO) under contract DE-AC36-08GO28308 with the National Renewable Energy Laboratory (NREL), operated by Alliance for Sustainable Energy, LLC. We thank Kristen Beckett for recording the PCHC NMR spectrum in $CDCl_3$. This work used Expanse at San Diego Supercomputer Center through allocation CTS120055 from the Advanced Cyberinfrastructure Coordination Ecosystem: Services & Support (ACCESS) program, which is supported by National Science Foundation grants #OAC-2138259, #OAC-2138286, #OAC-2138307, #OAC-2137603, and #OAC-2138296.

References

1 H. Zhang, S. Lin, H. Gao, K. Zhang, Y. Wang, Z. Zhou and W. Yi, *Commun. Chem.*, 2021, **4**, 81.
2 I. P. Beletskaya, C. Nájera and M. Yus, *Chem. Soc. Rev.*, 2020, **49**, 7101–7166.
3 L.-T. Wang, B. Zhou, F.-L. Liu, W.-T. Wei and L.-W. Ye, *Trends Chem.*, 2023, **5**, 906–919.
4 E. K. Reeves, E. D. Entz and S. R. Neufeldt, *Chem. – Eur. J.*, 2021, **27**, 6161–6177.
5 M. Bergmann, B. C. Almroth, S. M. Brander, T. Dey, D. S. Green, S. Gundogdu, A. Krieger, M. Wagner and T. R. Walker, *Science*, 2022, **376**, 469–470.
6 R. Geyer, J. R. Jambeck and K. L. Law, *Sci. Adv.*, 2017, **3**, e1700782.
7 S. C. Kosloski-Oh, Z. A. Wood, Y. Manjarrez, J. P. de los Rios and M. E. Fieser, *Mater. Horiz.*, 2021, **8**, 1084–1129.
8 G. W. Coates and Y. D. Y. L. Getzler, *Nat. Rev. Mater.*, 2020, **5**, 501–516.
9 M. Hong and E. Y.-X. Chen, *Green Chem.*, 2017, **19**, 3692–3706.
10 Polycarbonate Market Size, Share & Trends Report, 2030, **https://www.grandviewresearch.com/industry-analysis/polycarbonate-market**, (accessed May 18, 2024).
11 X.-B. Lu, W.-M. Ren and G.-P. Wu, *Acc. Chem. Res.*, 2012, **45**, 1721–1735.
12 G. W. Coates and D. R. Moore, *Angew. Chem., Int. Ed.*, 2004, **43**, 6618–6639.
13 M. Scharfenberg, J. Hilf and H. Frey, *Adv. Funct. Mater.*, 2018, **28**, 1704302.
14 G.-W. Yang, Y.-Y. Zhang and G.-P. Wu, *Acc. Chem. Res.*, 2021, **54**, 4434–4448.
15 D. J. Saxon, E. A. Gormong, V. M. Shah and T. M. Reineke, *ACS Macro Lett.*, 2021, **10**, 98–103.
16 M. I. Childers, J. M. Longo, N. J. Van Zee, A. M. LaPointe and G. W. Coates, *Chem. Rev.*, 2014, **114**, 8129–8152.
17 C. Li, R. J. Sablong, R. A. T. M. Van Benthem and C. E. Koning, *ACS Macro Lett.*, 2017, **6**, 684–688.
18 G.-P. Wu, W.-M. Ren, Y. Luo, B. Li, W.-Z. Zhang and X.-B. Lu, *J. Am. Chem. Soc.*, 2012, **134**, 5682–5688.
19 Y. Wang and D. J. Darensbourg, *Coord. Chem. Rev.*, 2018, **372**, 85–100.
20 G. S. Sulley, G. L. Gregory, T. T. D. Chen, L. Peña Carrodeguas, G. Trott, A. Santmarti, K.-Y. Lee, N. J. Terrill and C. K. Williams, *J. Am. Chem. Soc.*, 2020, **142**, 4367–4378.
21 Y. Liu, L.-M. Fang, B.-H. Ren and X.-B. Lu, *Macromolecules*, 2020, **53**, 2912–2918.
22 B. Schäffner, F. Schäffner, S. P. Verevkin and A. Börner, *Chem. Rev.*, 2010, **110**, 4554–4581.
23 J. H. Clements, *Ind. Eng. Chem. Res.*, 2003, **42**, 663–674.
24 M. North, R. Pasquale and C. Young, *Green Chem.*, 2010, **12**, 1514.
25 F. N. Singer, A. C. Deacy, T. M. McGuire, C. K. Williams and A. Buchard, *Angew. Chem., Int. Ed.*, 2022, **61**, e202201785.
26 Y. Yu, B. Gao, Y. Liu and X. Lu, *Angew. Chem., Int. Ed.*, 2022, **61**, e202204492.
27 T. M. McGuire, A. C. Deacy, A. Buchard and C. K. Williams, *J. Am. Chem. Soc.*, 2022, **144**, 18444–18449.

28 G. Rosetto, F. Vidal, T. M. McGuire, R. W. F. Kerr and C. K. Williams, *J. Am. Chem. Soc.*, 2024, **146**, 8381–8393.
29 Y. Yu, B.-H. Ren, Y. Liu and X.-B. Lu, *ACS Macro Lett.*, 2024, **13**, 1099–1104.
30 D. J. Darensbourg and S.-H. Wei, *Macromolecules*, 2012, **45**, 5916–5922.
31 W. C. Ellis, Y. Jung, M. Mulzer, R. Di Girolamo, E. B. Lobkovsky and G. W. Coates, *Chem. Sci.*, 2014, **5**, 4004.
32 Y. Xu, T. Zhang, Y. Zhou, D. Zhou, Z. Shen and L. Lin, *Polym. Degrad. Stab.*, 2019, **168**, 108957.
33 P. Nuss and M. J. Eckelman, *PLoS One*, 2014, **9**, e101298.
34 S. Hong and T. J. Marks, *Acc. Chem. Res.*, 2004, **37**, 673–686.
35 S. Seo, X. Yu and T. J. Marks, *J. Am. Chem. Soc.*, 2009, **131**, 263–276.
36 C. J. Barger, A. Motta, V. L. Weidner, T. L. Lohr and T. J. Marks, *ACS Catal.*, 2019, **9**, 9015–9024.
37 S. Schäfer, S. Kaufmann, E. S. Rösch and P. W. Roesky, *Chem. Soc. Rev.*, 2023, **52**, 4006–4045.
38 C. E. Kefalidis, L. Castro, L. Perrin, I. D. Rosal and L. Maron, *Chem. Soc. Rev.*, 2016, **45**, 2516–2543.
39 Y. Qiao and E. J. Schelter, *Acc. Chem. Res.*, 2018, **51**, 2926–2936.
40 H. Liu, S. Saha and M. S. Eisen, *Coord. Chem. Rev.*, 2023, **493**, 215284.
41 V. L. Weidner, C. J. Barger, M. Delferro, T. L. Lohr and T. J. Marks, *ACS Catal.*, 2017, **7**, 1244–1247.
42 C. J. Barger, R. D. Dicken, V. L. Weidner, A. Motta, T. L. Lohr and T. J. Marks, *J. Am. Chem. Soc.*, 2020, **142**, 8019–8028.
43 Y.-M. Tu, F.-L. Gong, Y.-C. Wu, Z. Cai and J.-B. Zhu, *Nat. Commun.*, 2023, **14**, 3198.
44 L. Wursthorn, K. Beckett, J. O. Rothbaum, R. M. Cywar, C. Lincoln, Y. Kratish and T. J. Marks, *Angew. Chem., Int. Ed.*, 2023, **62**, e202212543.
45 L. Ye, X. Liu, K. B. Beckett, J. O. Rothbaum, C. Lincoln, L. J. Broadbelt, Y. Kratish and T. J. Marks, *Chem*, 2024, **10**, 172–189.
46 J. O. Rothbaum, A. Motta, Y. Kratish and T. J. Marks, *J. Am. Chem. Soc.*, 2022, **144**, 17086–17096.
47 A. Schäfer, H. Horn and R. Ahlrichs, *J. Chem. Phys.*, 1992, **97**, 2571–2577.
48 F. Weigend and R. Ahlrichs, *Phys. Chem. Chem. Phys.*, 2005, **7**, 3297–3305.
49 J. P. Perdew, M. Ernzerhof and K. Burke, *J. Chem. Phys.*, 1996, **105**, 9982–9985.
50 C. Adamo and V. Barone, *J. Chem. Phys.*, 1999, **110**, 6158–6170.
51 S. Grimme, S. Ehrlich and L. Goerigk, *J. Comput. Chem.*, 2011, **32**, 1456–1465.
52 S. Grimme, J. Antony, S. Ehrlich and H. Krieg, *J. Chem. Phys.*, 2010, **132**, 154104.
53 A. V. Marenich, C. J. Cramer and D. G. Truhlar, *J. Phys. Chem. B*, 2009, **113**, 6378–6396.
54 C. T. Campbell and J. R. V. Sellers, *J. Am. Chem. Soc.*, 2012, **134**, 18109–18115.
55 B. E. Leonhardt, M. Head-Gordon and A. T. Bell, *ACS Catal.*, 2024, **14**, 3049–3064.
56 J. Ariai and U. Gellrich, *Phys. Chem. Chem. Phys.*, 2023, **25**, 14005–14015.